Supplementary Material

High molecular weight SOA formation during limonene ozonolysis: Insights from ultrahigh-resolution FT-ICR mass spectrometry characterization

S. Kundu[1,2], R. Fisseha[3], A. L. Putman[3], T. A. Rahn[3], and L. R. Mazzoleni[1,2*]

[1]Department of Chemistry, Michigan Technological University, Houghton, MI 49931, USA

[2]Atmospheric Science Program, Michigan Technological University, Houghton, MI 49931, USA

[3]Earth and Environmental Sciences, Los Alamos National Laboratory, Los Alamos, NM 87545, USA

*Corresponding author phone: +1-906-487-1853; fax: +1-906-487-2061; e-mail: lrmazzol@mtu.edu

Figure S1. Superimposition of the data from replicate analyses of an aerosol extract. Mixture of acetonitrile and water (1:1) is used as solvent. The symbol sizes represent the relative abundances of the chemical formulas. The higher is the size of symbol, the higher is the relative abundances. A majority of the data overlay well in terms of chemical identity and relative abundances. However, there are unique formulas between the replicate analyses. Also, the relative abundances of identical chemical formulas from the replicate analyses are not similar in some cases.

Figure S2. Superimposition of the data from aerosol samples from two different experiments. Relative humidity was maintained at 0% and 4% in the experiments. Other experimental conditions were identical. Mixture of acetonitrile and water is used as solvent. The symbol sizes represent the relative abundances of the chemical formulas. The higher is the size of symbol, the higher is the relative abundances. A majority of the data overlay well in terms of chemical identity and relative abundances. However, there are unique formulas between the aerosol samples. Also, the relative abundances of identical chemical formulas from two aerosol samples are not similar in some cases.

Figure S3. Averaged ESI FT-ICR negative ion mass spectra of acetonitrile and water (1:1) extracted aerosol sample from the ozonolysis of limonene. Four characteristic regions at 140 <m/z <300, 300 <m/z < 500, 500 <m/z < 700 and 700 <m/z < 850 were observed.

Figure S4a. Schematic of the formation of a CH_2-homologous series with double bond equivalents (DBE) 4. Alkoxy radical (XVIII) resulting from the limonene ozonolysis is converted to another alkoxy radical (XIX) with one more oxygen atom via oxygen-increasing-reactions (OIR) (isomerization→ O_2→ RO_2).The number in parenthesis beside OIR indicates the repetition of OIR sequence. Cleavage of the alkoxy radical (XIX) followed by reactions with O_2 and RO_2 and OIR (1) reactions can form neutral molecule (XXI). Reaction with RO_2 with the alkoxy radical (XX) followed by the ozonolysis to the exocyclic double bond form a neutral molecule (XXII).Repetition of the OIR steps on (XIX) forms an alkoxy radical, which is converted to a neutral molecule (XXIII).Organic aerosol formation with C_{11}-C_{12} carbon occurs by the reactive absorption of gas phase organics (e.g., glyoxal) on aerosols as shown in the box.

Figure S4b. Schematic of the formation of O-homologous series with double bond equivalents (DBE) 4. Alkoxy radical (XXIV) resulting from the limonene ozonolysis is converted to another alkoxy radical (XXV) with one more oxygen atom via oxygen-increasing-reactions (OIR) (isomerization → O_2→ RO_2). Repetitions of the OIR steps on this radical forms alkoxy radicals such as XXVI, XXVII, XXVIII and XXIX. The number in parenthesis beside OIR indicates the repetition of OIR sequence. Neutral molecules are formed from these alkoxy radical to form homologous series.

Figure S5. The change of double bond equivalents (DBE) by 2 in (a) Criegee reaction pathway; Criegee radicals react with neutral molecules with the formation of peroxide ester and ozonide (b) hydroperoxide reaction pathway; hydroperoxides react with neutral molecules and (c) hemi-acetal pathway, carbonyl compounds react with alcohols. All the participating building units shown are highly dominant in the mass spectra. The resulting accretion products are also the most dominant in the mass spectra. See the Table S1.

Figure S6. The change of double bond equivalents (DBE) by both 3 and 2 in (a) aldol condensation reaction pathway; reactions occur between carbonyl compounds and (b) esterification reaction pathway; reactions occur between carboxylic acids and alcohols. Water molecule can be eliminated in these reactions. All the participating building units and resulting oligomers are dominant in the mass spectra. See Table S1.

Figure S7. Reconstructed product ion spectra of the precursor peaks at the m/z of (a) 185, (b) 357, (c) 387, (d) 417, and (e) 541. Fragmentation was carried out using infrared multiphoton dissociation (IRMPD) technique. A normalized energy level of 100% was applied with an isolation width of 2 m/z units. Reconstruction of the mass spectrum was done following the co-addtion of ~50 transients and formula assignments with a formula calculator (Composer, Sierra Analytics). The spectra show only the monoisotopic peaks. The inset shows the fragmentation processes and potential building units of each of the reaction channels that could form the prominent isobaric ions (shown in the inset) of the precursors.

Table S2. Formation of high abundance Group III compounds in the mass spectra. They are identified following different formation processes of high MW compounds.

Theoretical neutral mass	Chemical formula	Peak intensity (%)[a]	Hydroperoxide reaction[b]	Criegee reaction[c]	Hemi-acetal reaction[d]	Condensation reaction[e]
528.2571	$C_{26}H_{40}O_{11}$	4	2	4	4	2
542.2727	$C_{27}H_{42}O_{11}$	5	4	6	4	10
544.252	$C_{26}H_{40}O_{12}$	6	5	1	7	3
546.2676	$C_{26}H_{42}O_{12}$	5	3	1	6	2
556.2884	$C_{28}H_{44}O_{11}$	5	4	2	5	2
558.2676	$C_{27}H_{42}O_{12}$	8	4	1	6	4
560.2469	$C_{26}H_{40}O_{13}$	6	3	3	5	6
560.2833	$C_{27}H_{44}O_{12}$	6	2	2	5	2
562.2625	$C_{26}H_{42}O_{13}$	5	4	1	6	3
572.2469	$C_{27}H_{40}O_{13}$	5	4	2	6	7
572.2833	$C_{28}H_{44}O_{12}$	8	5	1	6	3
574.2625	$C_{27}H_{42}O_{13}$	9	4	1	6	6
574.2989	$C_{28}H_{46}O_{12}$	6	4	2	6	1
576.2418	$C_{26}H_{40}O_{14}$	4	3	1	7	5
576.2782	$C_{27}H_{44}O_{13}$	7	2	1	4	3
586.2625	$C_{28}H_{42}O_{13}$	6	3	1	5	8
586.2989	$C_{29}H_{46}O_{12}$	6	3	2	6	2
588.2782	$C_{28}H_{44}O_{13}$	11	9	5	12	22
590.2575	$C_{27}H_{42}O_{14}$	8	1	2	3	6
590.2938	$C_{28}H_{46}O_{13}$	7	3	×	3	2
592.2731	$C_{27}H_{44}O_{14}$	6	3	1	×	4
600.2782	$C_{29}H_{44}O_{13}$	5	4	1	7	8
602.2575	$C_{28}H_{42}O_{14}$	6	2	2	4	8
602.2938	$C_{29}H_{46}O_{13}$	9	2	3	3	4
604.2731	$C_{28}H_{44}O_{14}$	11	3	1	6	6
604.3095	$C_{29}H_{48}O_{13}$	6	2	2	7	2
606.2524	$C_{27}H_{42}O_{15}$	5	3	2	5	7
606.2888	$C_{28}H_{46}O_{14}$	7	2	2	4	4
616.2731	$C_{29}H_{44}O_{14}$	6	4	1	10	7
616.3095	$C_{30}H_{48}O_{13}$	5	2	1	4	3
618.2524	$C_{28}H_{42}O_{15}$	5	2	1	7	7
618.2888	$C_{29}H_{46}O_{14}$	10	2	1	4	5
620.268	$C_{28}H_{44}O_{15}$	7	2	3	4	7
620.3044	$C_{29}H_{48}O_{14}$	6	3	1	8	3
622.2837	$C_{28}H_{46}O_{15}$	5	6	1	7	5
632.268	$C_{29}H_{44}O_{15}$	5	4	1	9	10
632.3044	$C_{30}H_{48}O_{14}$	6	2	1	6	4
634.2837	$C_{29}H_{46}O_{15}$	8	4	1	9	7
636.2993	$C_{29}H_{48}O_{15}$	5	4	×	6	3
648.2993	$C_{30}H_{48}O_{15}$	5	2	2	3	6

[a]It is calculated with respect to the base peak in the mass spectra.

[b]The number of possible combinations between two hydroperoxides and a neutral molecule.

[c]The number of possible combinations between two Criegee radicals and a neutral molecule.

[d]The number of possible combinations between three neutral molecules.

[e]The number of possible combinations between three neutral molecules with elimination of two molecules of water by aldol condensation and esterification reactions.

Figure S1.

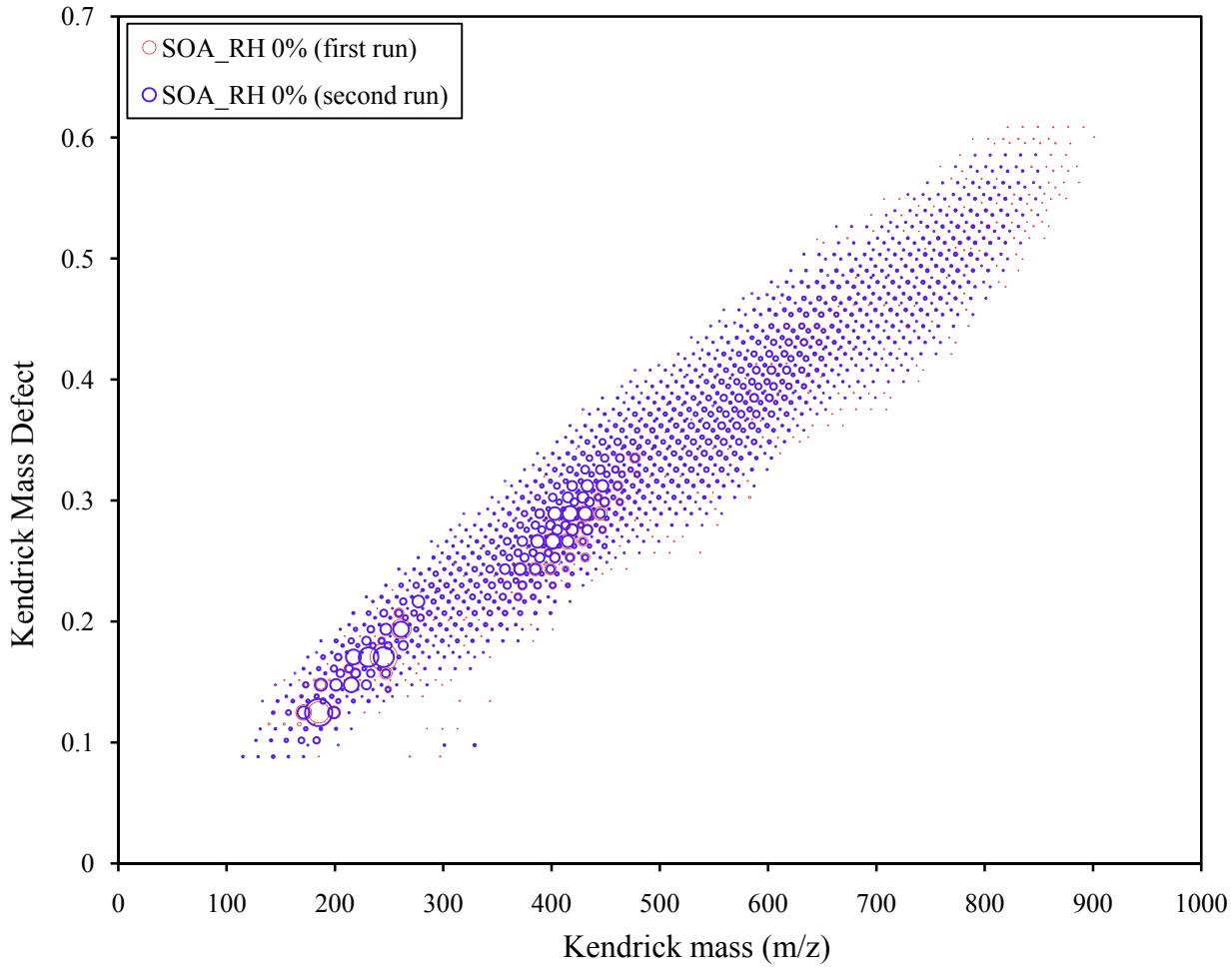
SOA_RH 0% (first run)
SOA_RH 0% (second run)
Kendrick Mass Defect
Kendrick mass (m/z)
0
0.1
0.2
0.3
0.4
0.5
0.6
0.7
0
100
200
300
400
500
600
700
800
900
1000

Figure S2.

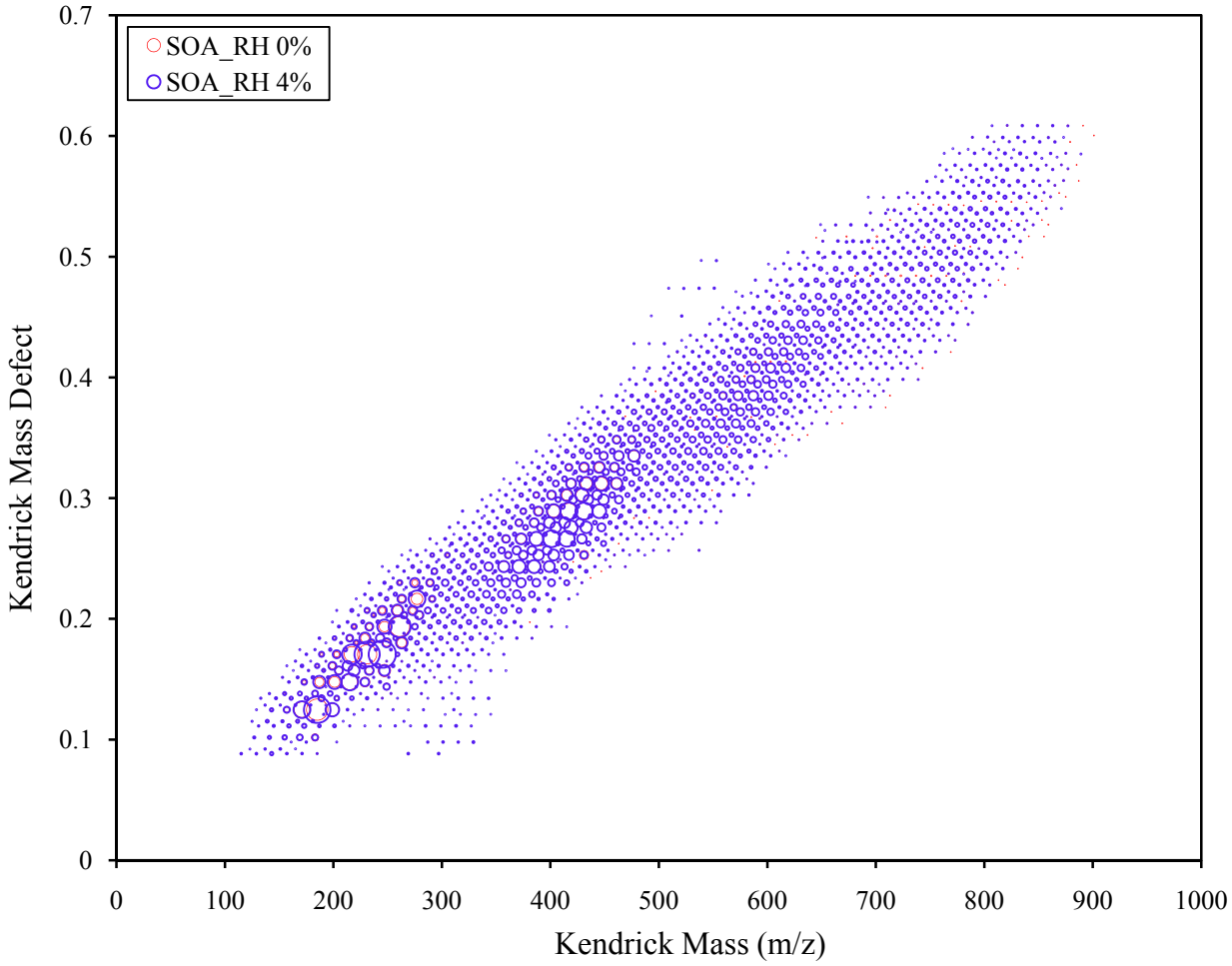
SOA_RH 0%
SOA_RH 4%
Kendrick Mass Defect
Kendrick Mass (m/z)
0
0.1
0.2
0.3
0.4
0.5
0.6
0.7
0
100
200
300
400
500
600
700
800
900
1000

Figure S3.

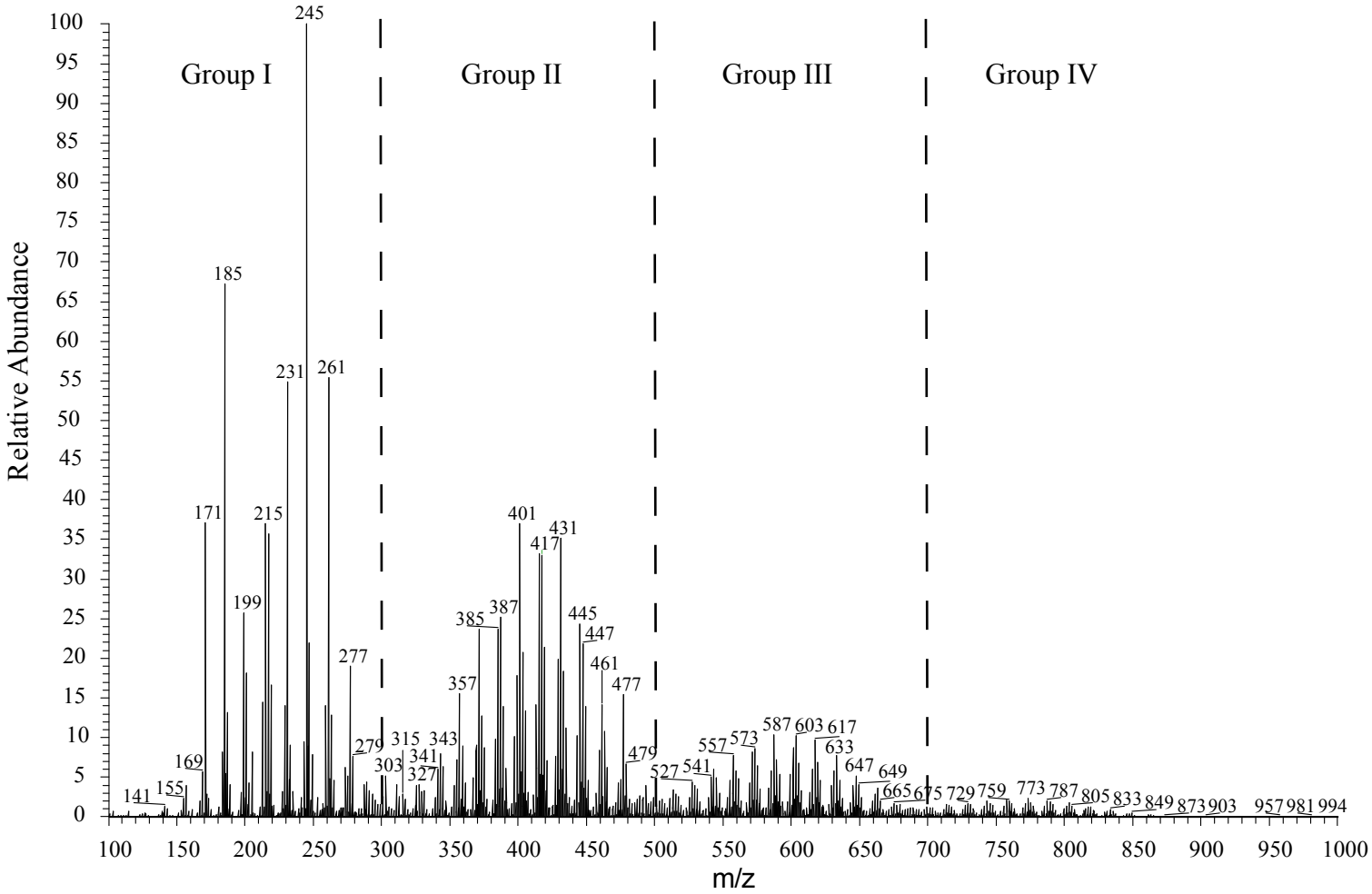
Group I
Group II
Group III
Group IV
Relative Abundance
m/z
245
185
231
261
171
215
199
277
401
431
417
385
387
445
447
461
477
357
279
315
343
303
341
327
479
527
541
557
573
587
603
617
633
647
649
665
675
729
759
773
787
805
833
849
873
903
957
981
994
141
155
169

Figure S4a.

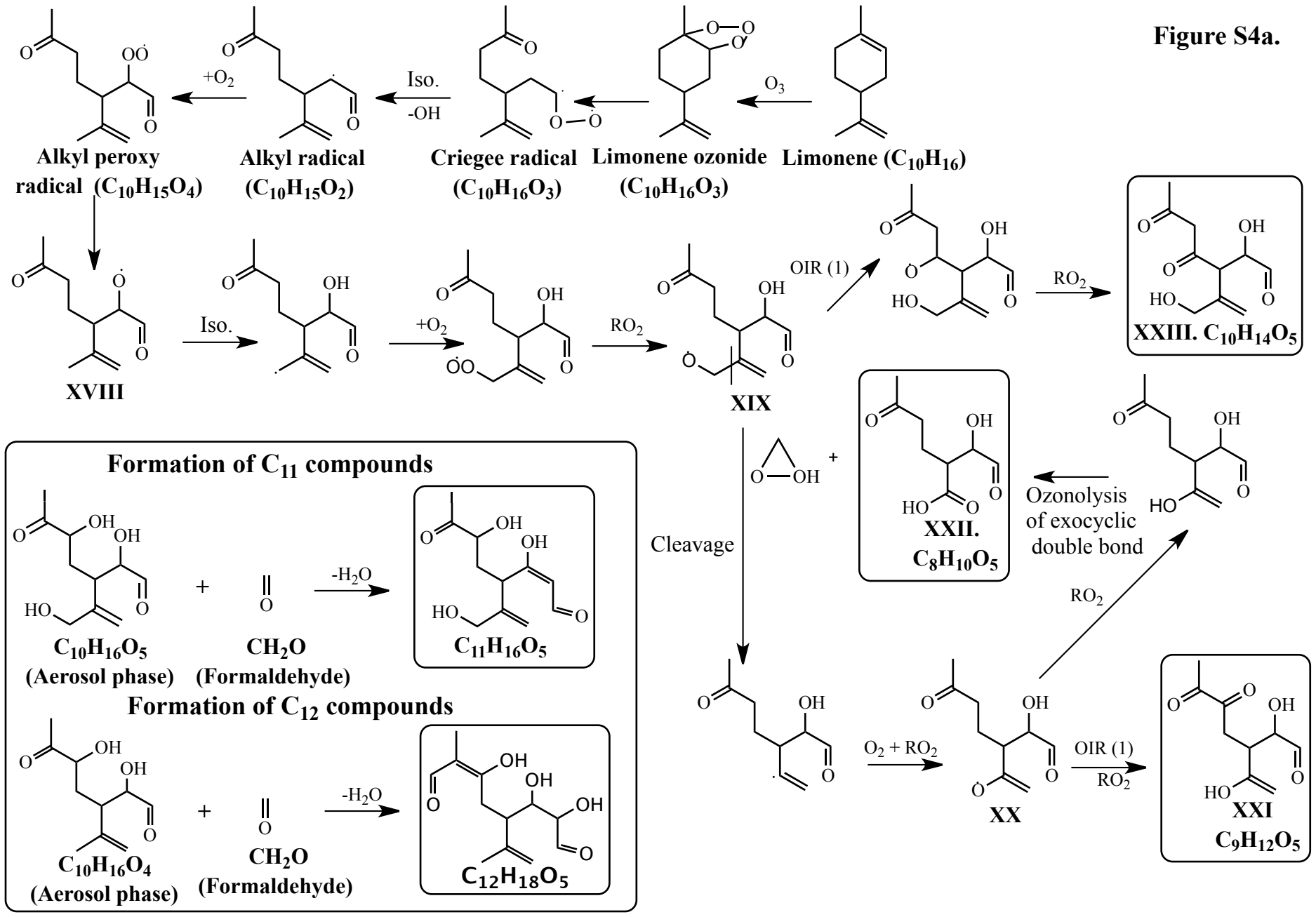
Limonene ($C_{10}H_{16}$)
O_3
Limonene ozonide ($C_{10}H_{16}O_3$)
Criegee radical ($C_{10}H_{16}O_3$)
Iso.
-OH
Alkyl radical ($C_{10}H_{15}O_2$)
$+O_2$
Alkyl peroxy radical ($C_{10}H_{15}O_4$)
XVIII
Iso.
$+O_2$
RO_2
XIX
OIR (1)
RO_2
XXIII. $C_{10}H_{14}O_5$
Cleavage
Ozonolysis of exocyclic double bond
XXII. $C_8H_{10}O_5$
$O_2 + RO_2$
OIR (1)
RO_2
XX
XXI
$C_9H_{12}O_5$
Formation of C_{11} compounds
$C_{10}H_{16}O_5$ (Aerosol phase)
CH_2O (Formaldehyde)
$-H_2O$
$C_{11}H_{16}O_5$
Formation of C_{12} compounds
$C_{10}H_{16}O_4$ (Aerosol phase)
CH_2O (Formaldehyde)
$-H_2O$
$C_{12}H_{18}O_5$

Figure S4b.

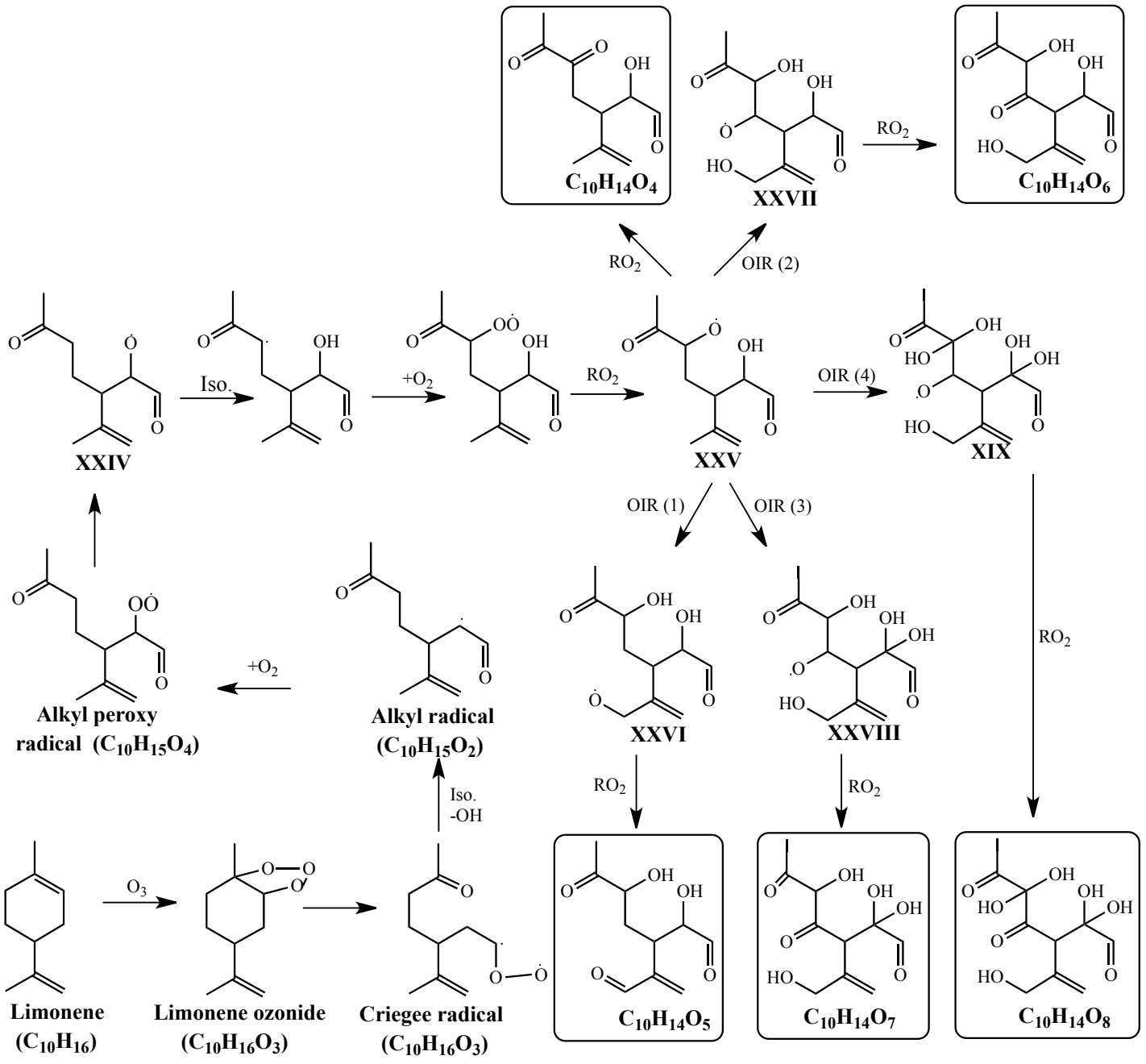
Limonene
(C10H16)
O3
Limonene ozonide
(C10H16O3)
Criegee radical
(C10H16O3)
Iso.
-OH
Alkyl radical
(C10H15O2)
+O2
Alkyl peroxy
radical (C10H15O4)
Iso.
+O2
RO2
XXIV
XXV
OIR (1)
OIR (3)
OIR (2)
OIR (4)
XXVI
XXVIII
XIX
XXVII
C10H14O4
C10H14O5
C10H14O6
C10H14O7
C10H14O8
RO2
RO2
RO2
RO2
RO2

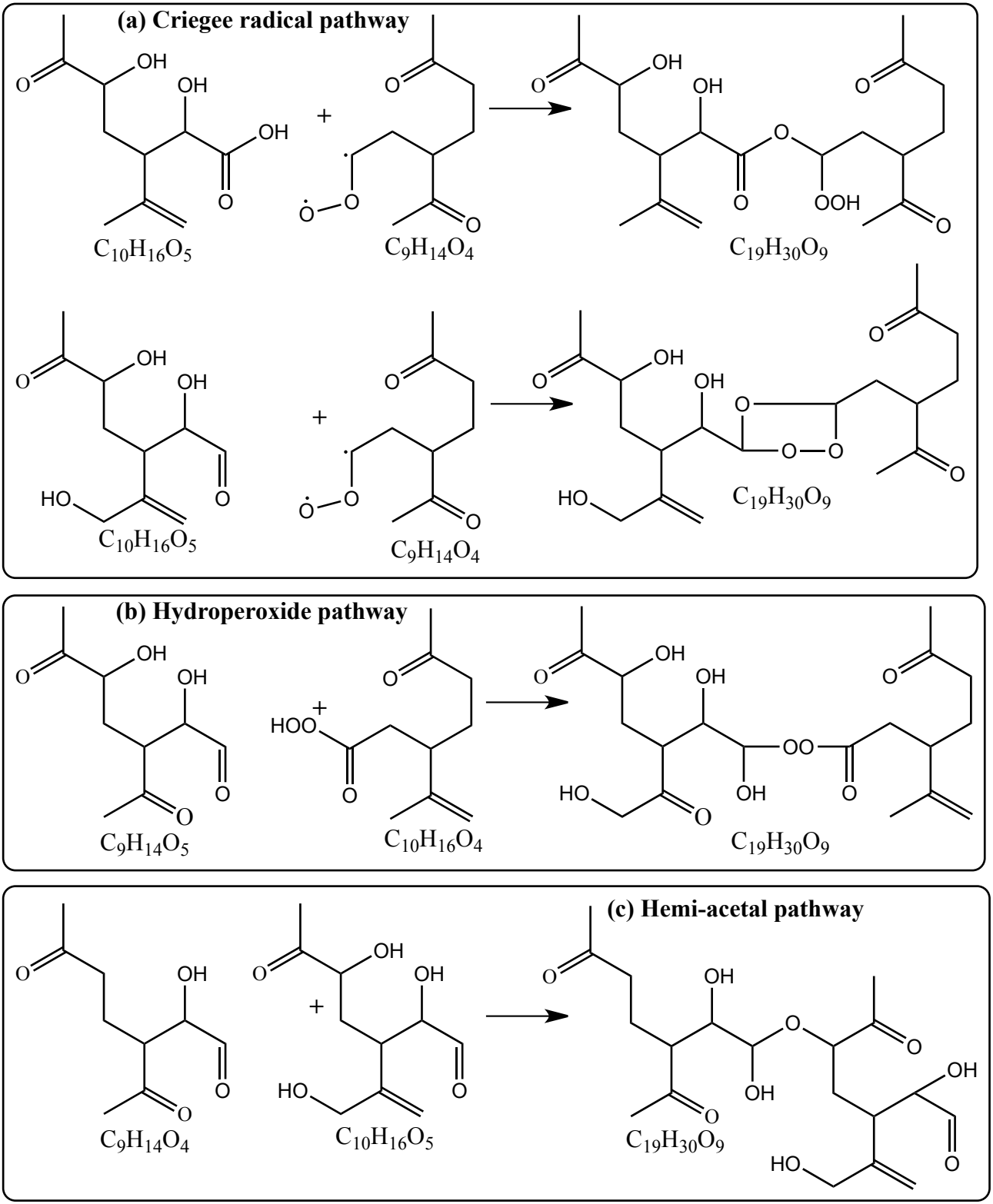
(a) Criegee radical pathway
C10H16O5
C9H14O4
C19H30O9
C10H16O5
C9H14O4
C19H30O9
(b) Hydroperoxide pathway
C9H14O5
C10H16O4
C19H30O9
(c) Hemi-acetal pathway
C9H14O4
C10H16O5
C19H30O9

Figure S6.

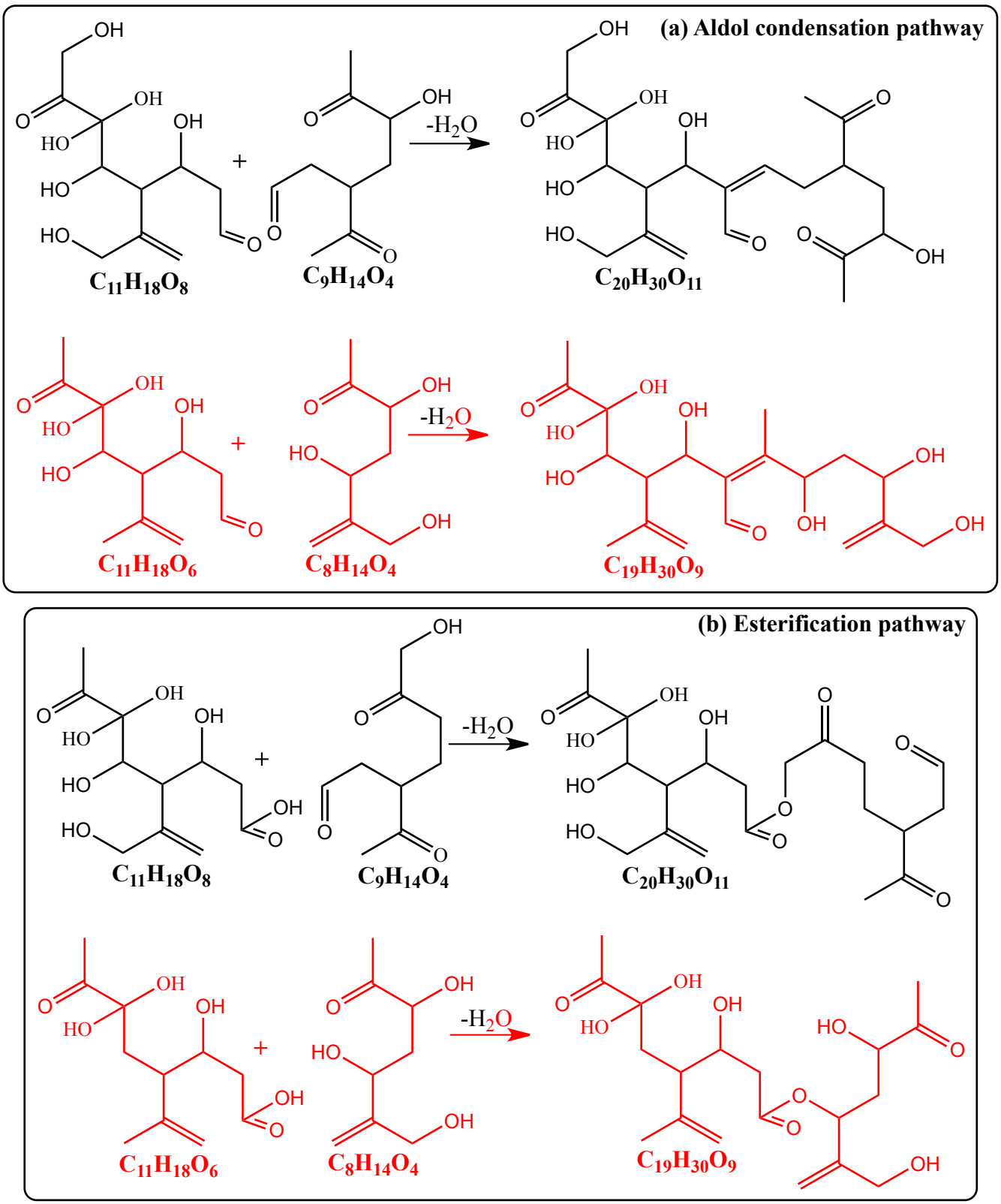
(a) Aldol condensation pathway
-H2O
C11H18O8
C9H14O4
C20H30O11
C11H18O6
C8H14O4
C19H30O9
(b) Esterification pathway
-H2O
C11H18O8
C9H14O4
C20H30O11
C11H18O6
C8H14O4
C19H30O9

Figure S7.

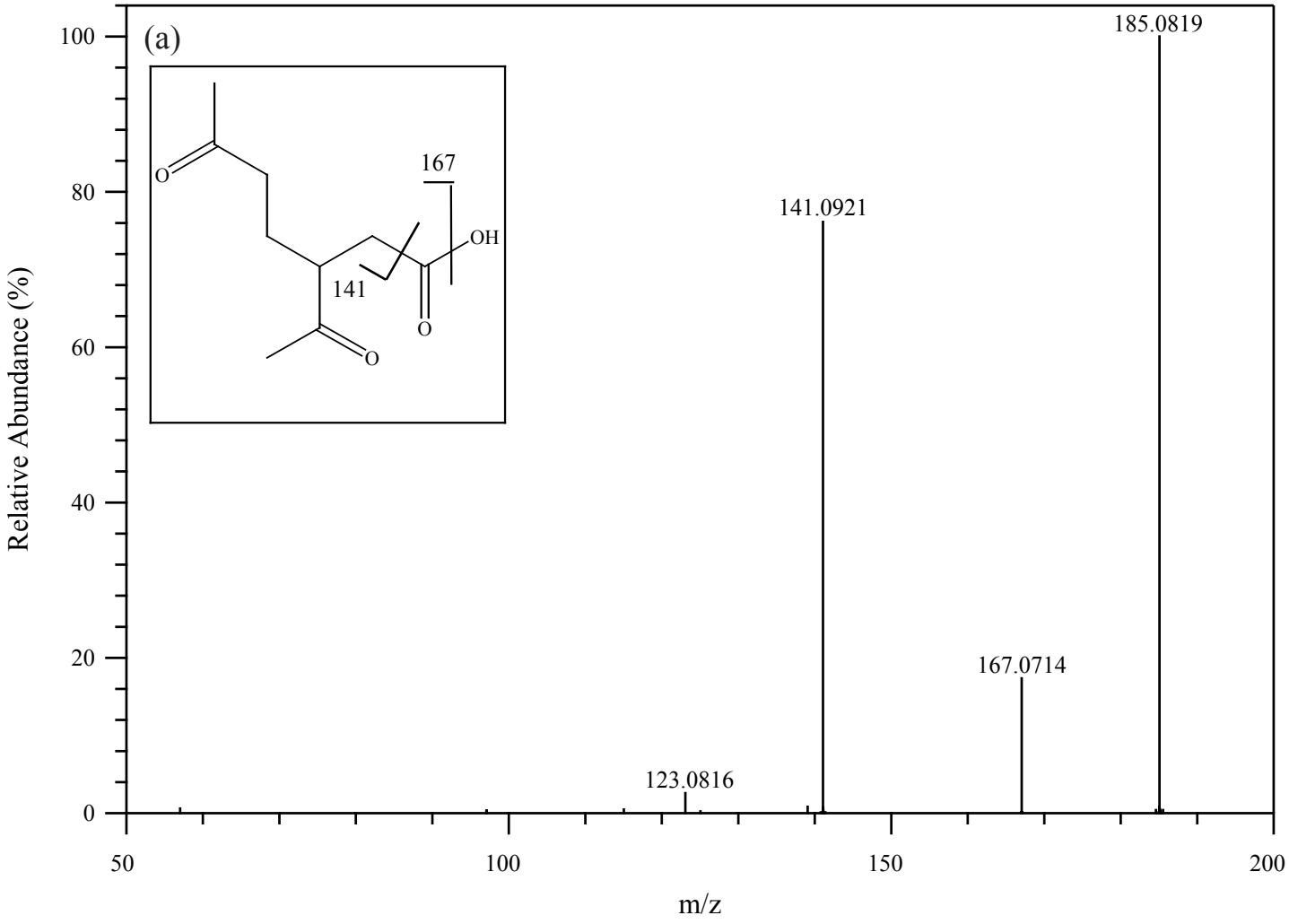
(a)
185.0819
141.0921
167.0714
123.0816
167
141
OH
O
O
O
Relative Abundance (%)
m/z
0
20
40
60
80
100
50
100
150
200

Figure S7.

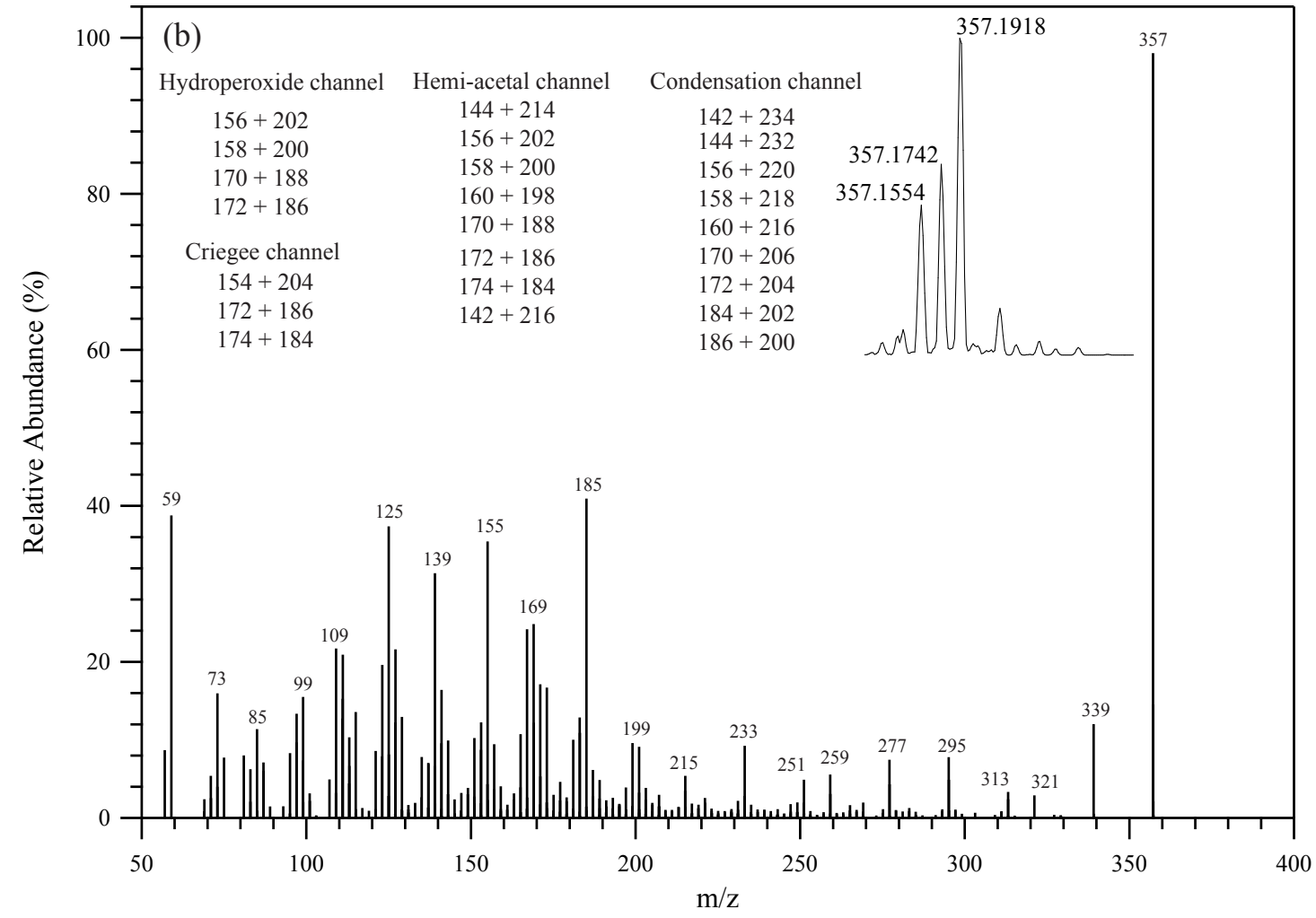
(b)
Hydroperoxide channel
156 + 202
158 + 200
170 + 188
172 + 186
Criegee channel
154 + 204
172 + 186
174 + 184
Hemi-acetal channel
144 + 214
156 + 202
158 + 200
160 + 198
170 + 188
172 + 186
174 + 184
142 + 216
Condensation channel
142 + 234
144 + 232
156 + 220
158 + 218
160 + 216
170 + 206
172 + 204
184 + 202
186 + 200
357.1918
357
357.1742
357.1554
Relative Abundance (%)
m/z

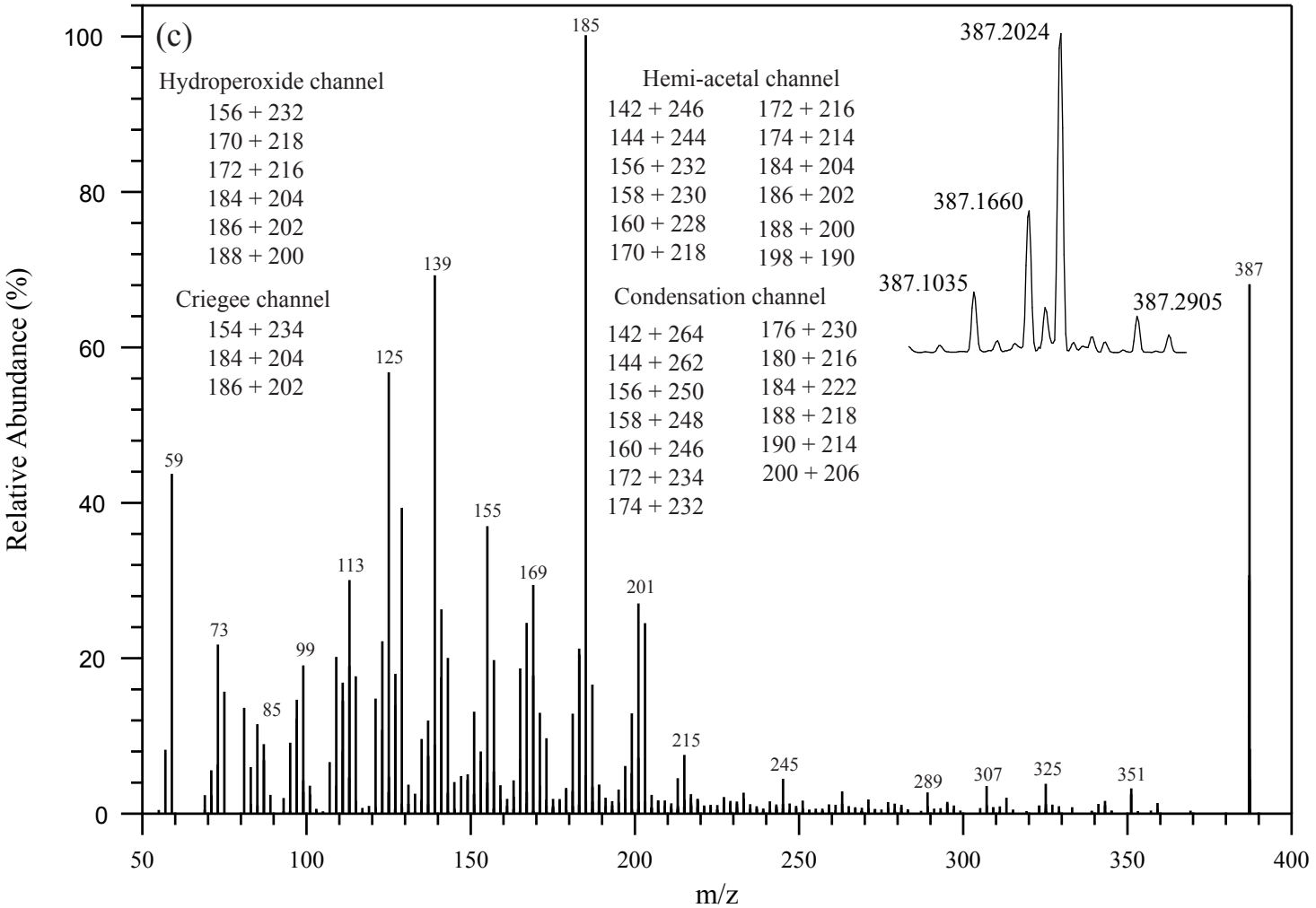
(c)
Hydroperoxide channel
156 + 232
170 + 218
172 + 216
184 + 204
186 + 202
188 + 200
Criegee channel
154 + 234
184 + 204
186 + 202
Hemi-acetal channel
142 + 246
144 + 244
156 + 232
158 + 230
160 + 228
170 + 218
172 + 216
174 + 214
184 + 204
186 + 202
188 + 200
198 + 190
Condensation channel
142 + 264
144 + 262
156 + 250
158 + 248
160 + 246
172 + 234
174 + 232
176 + 230
180 + 216
184 + 222
188 + 218
190 + 214
200 + 206
387.2024
387.1660
387.1035
387.2905
387
Relative Abundance (%)
m/z

Figure S7.

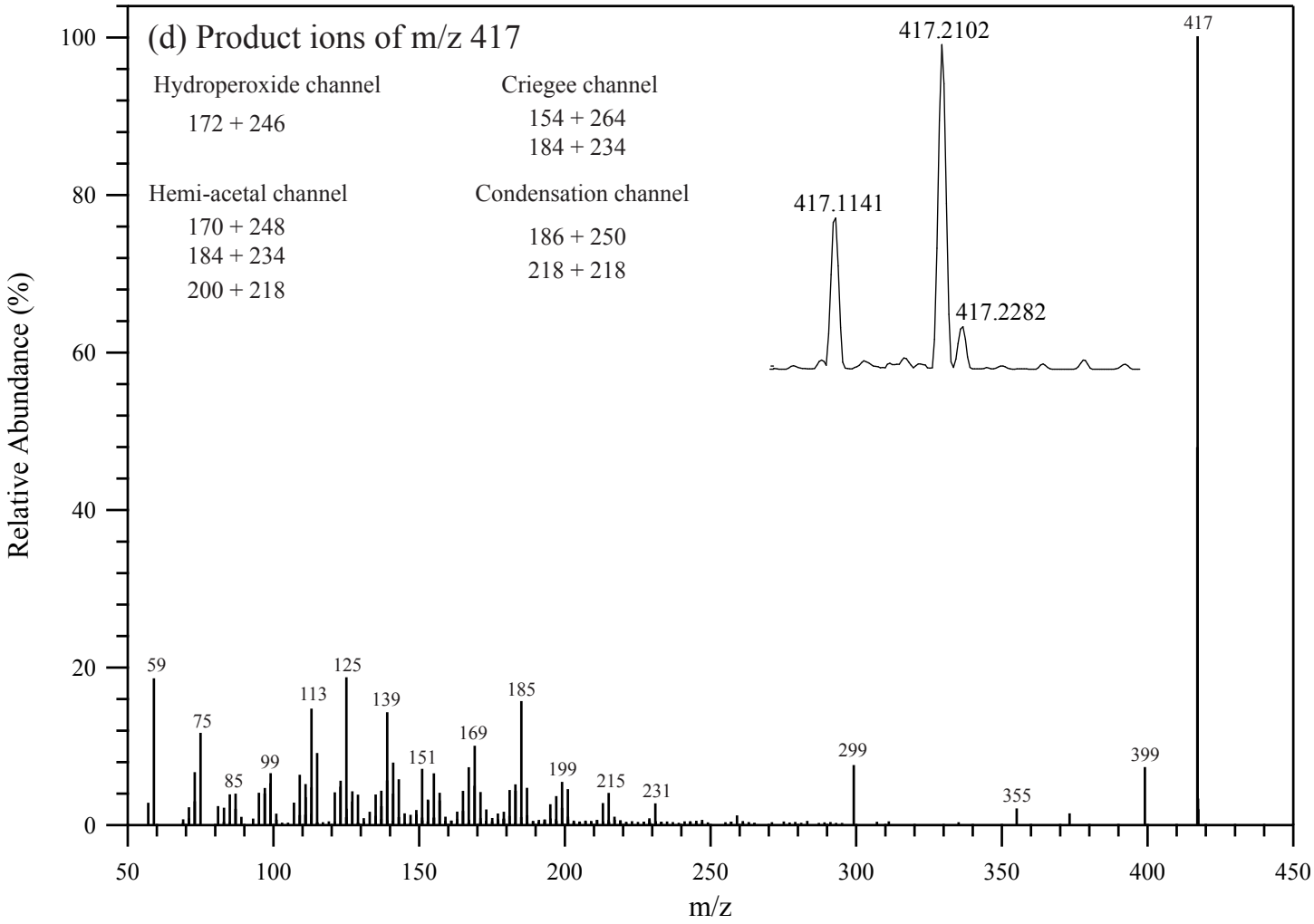
(d) Product ions of m/z 417
Hydroperoxide channel
172 + 246
Criegee channel
154 + 264
184 + 234
Hemi-acetal channel
170 + 248
184 + 234
200 + 218
Condensation channel
186 + 250
218 + 218
417.2102
417
417.1141
417.2282
Relative Abundance (%)
m/z

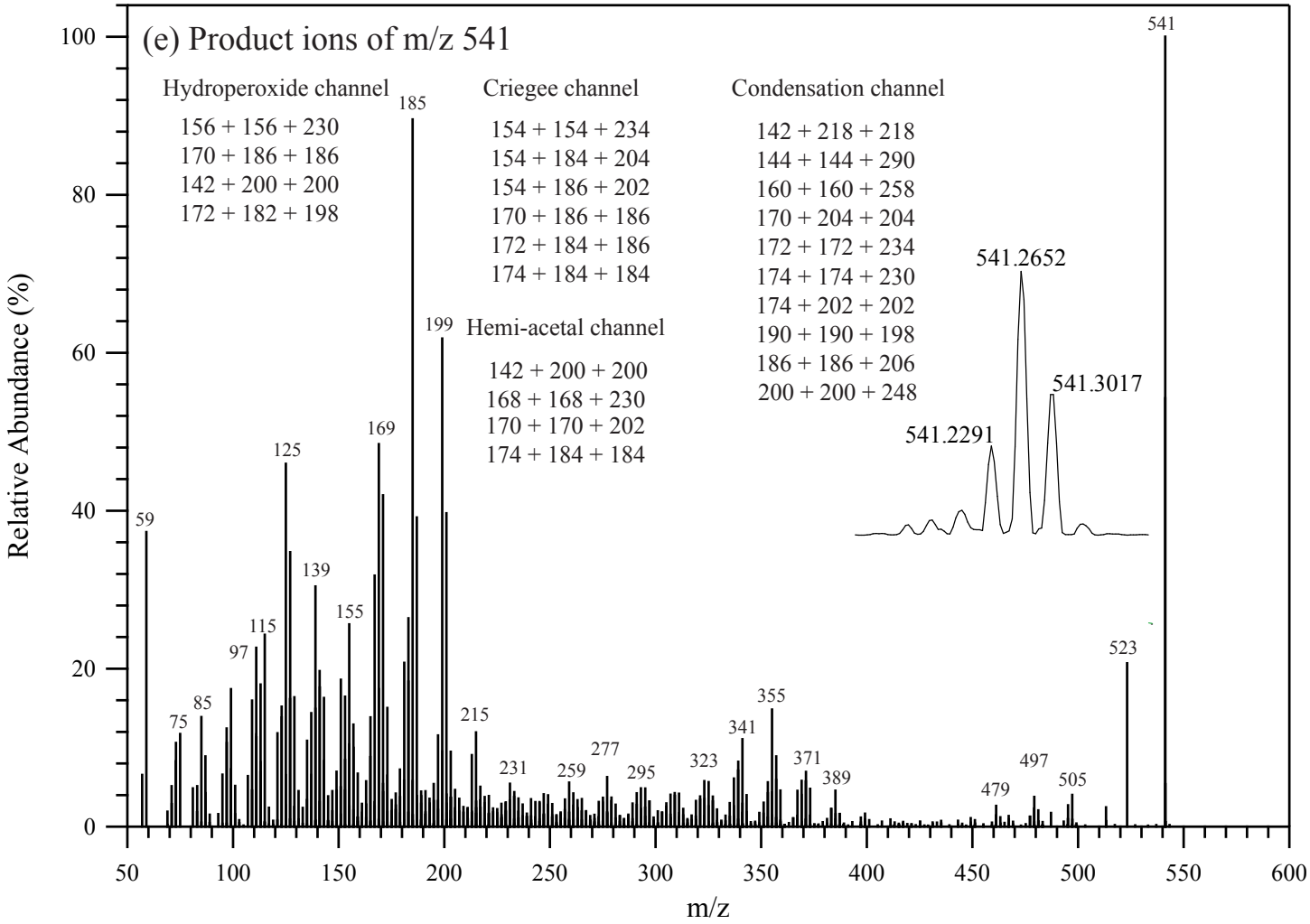
(e) Product ions of m/z 541
Hydroperoxide channel
156 + 156 + 230
170 + 186 + 186
142 + 200 + 200
172 + 182 + 198
Criegee channel
154 + 154 + 234
154 + 184 + 204
154 + 186 + 202
170 + 186 + 186
172 + 184 + 186
174 + 184 + 184
Hemi-acetal channel
142 + 200 + 200
168 + 168 + 230
170 + 170 + 202
174 + 184 + 184
Condensation channel
142 + 218 + 218
144 + 144 + 290
160 + 160 + 258
170 + 204 + 204
172 + 172 + 234
174 + 174 + 230
174 + 202 + 202
190 + 190 + 198
186 + 186 + 206
200 + 200 + 248
541.2652
541
541.3017
541.2291
Relative Abundance (%)
m/z